Formation of calcium phosphate nanostructures under the influence of self-assembling hybrid elastin-like-statherin recombinamers

M. Hamed Misbah, M. Espanol, Luis Quintanilla, M. P. Ginebra and J. Carlos Rodríguez-Cabello

1. Introduction

The synthesis of self-assembled calcium phosphate hybrid structures represents a novel approach for the fabrication a new class of materials. In self-assembly processes, non-covalent cooperative interactions are responsible for the aggregation and formation of supramolecular structures with unique properties.[1–3] In the particular field of calcium phosphates, self-assembly represents a major tool for understanding bone mineralization and the basis to create new functional materials. In this process, organic molecules with different amphiphilic properties regulate the organization of different organic/inorganic hybrid structures, thus controlling the biomimetic mineralization process.[1,2,4,5] They can be introduced as insoluble additive (templating approach) like is the case of Langmuir monolayers and self-assembled monolayers that are used to determine the functional group distance to nucleate a desired mineral phase or even to control the growth of particular polymorphs.[4,6–8] Alternatively, organic molecules can also be used as soluble additives imparting great influence on crystallization modulating the morphology, size and polymorph type of the crystal.[4,9,10] The abilities of organic molecules to complex ions, self-aggregate or adsorb onto specific crystal surfaces are just some strategies through which soluble molecules control mineralization.

Various types of organic molecules have been used to investigate the organization of the organic/inorganic hybrid structures, to help understanding the mechanisms controlling the biomimetic mineralization processes.[1,2,4,5] For example, self-assembled peptide-amphiphile can direct hydroxyapatite (HA) to form a composite material with an organization similar to that found for collagen fibrils and HA in bone.[1,2] Furthermore, diblock copolymers can induce *meso*-skeleton formation of interconnected calcium phosphate nanofibres with a star/neuron-like morphology, although more complex nested forms can also be produced.[2,5] Identical structures have also been generated using simpler organic molecules such as surfactants, sodium polyacrylate and poly(diallyldimethylammonium chloride).[9] Also, studies using dephosphorylated fluorenylmethyloxycarbonyl (Fmoc) tyrosine phosphate had demonstrated the capability of spontaneously forming fibres that could later be mineralized.[11]

Elastin-like polypeptides and, now-a-days, their recombinant versions, elastin-like recombinamers (ELRs) are a family of polypeptides inspired by natural elastin that can be used to control the biomimetic mineralization process.[12] They are composed of simple amino-acid sequences $(VPGXG)^a$ (see Table 1 for details on sample nomenclature), where X can be any natural or synthetic amino acid except proline.[13–15] In aqueous

Table 1 Amino acid sequence of the ELRs

ELR name	ELR amino acid sequence[a]	M_w (kDa)
E50I60	MESLLP[((VPGVG)$_2$(VPGEG)(VPGVG)$_2$)$_{10}$](VGIPG)$_{60}$V	46 999 ± 19.96
(SN$_A$15)$_3$E50I60	MESLLPV(DDDEEKFLRRIGRFG)$_3$[((VPGVG)$_2$(VPGEG) (VPGVG)$_2$)$_{10}$](VGIPG)$_{60}$V	52 970 ± 12
(IK)24	MESLLP[[(VPGIG)$_2$(VPGKG)(VPGIG)$_2$]$_{24}$V	51 996.5 ± 11.30
((IK)2-SN$_A$15-(IK)2)3	MESLLP[[(VPGIG)$_2$(VPGKG)(VPGIG)$_2$]$_2$DDDEEKFLRRIGRFG[(VPGIG)$_2$(VPGKG) (VPGIG)$_2$]$_2$]$_3$V	31 857

[a] D ¼ L-aspartic, E ¼ L-glutamic, K ¼ L-lysine, F ¼ L-phenylalanine, L ¼ L-leucine, R ¼ L-arginine, I ¼ L-isoleucine, G ¼ glycine, V ¼ L-valine, P ¼ L-proline, M ¼ L-methionine and S ¼ L-serine.

solution, ELRs exhibit an intrinsic inverse transition temperature (T_t). Below T_t, the free chains remain disordered and have random coil conformations that are fully hydrated as a result of hydrophobic hydration. This hydration around hydrophobic moieties is ordered into cage-like or clathrate structures that are stabilized by hydrogen bonding. In contrast, above T_t the ELR backbone is dehydrated and can self-assemble into β-turn conformations.[13–15] In this structure, intra- and inter-chain hydrophobic contacts result in formation of a phase-separated state. The guest amino acid residue (X) can be varied to change the value of T_t and, consequently, the amphiphilic properties of the designed ELR block.[13,16] For example, poly (VPGIG) exhibits a hydrophobic nature stemming from the presence of L-isoleucine (I) as guest.[16,17] In contrast, poly(VPGEG) and poly(VPGKG) exhibit a hydrophilic nature due to the presence of L-glutamic (E) acid and L-lysine (K), respectively.[16,18]

The above simple ELR-based blocks can be combined with each other to make amphiphilic ELRs that can self-assemble and generate different nanostructures.[3,19] For example, the ELR E50I60 is composed of an I60 block ((VGIPG)$_{60}$V) with a T_t of about 19 °C and an E50 block (MESLLP[(VPGVG)$_2$(VPGEG)(VPGVG)$_2$)$_{10}$) whose estimated T_t is higher than 100 °C at neutral pH.[3,18,20] The chains of this ELR can self-assemble into micelles in which the hydrophobic I60 blocks form the core and the hydrophilic E50 blocks the corona. In contrast, the ELR IK24 (MESLLP[[(VPGIG)$_2$ (VPGKG)(VPGIG)$_2$]$_{24}$V) cannot form a micellar structure above its T_t of 31.5 °C.[19] The chain of this ELR is composed of hydrophobic (VPGIG)$_2$ and hydrophilic (VPGKG) blocks.

Such biocompatible ELRs could be used as a regenerative material in various applications, such as bone regeneration, when recombined with a bioactive domain.[12] This domain could, for example, be the hydrated N-terminal 15-amino-acid residue of salivary statherin known as SN15 (DS$_P$S$_P$-EEKFLRRIGRFG), or its analog SN$_A$15 (DDDEEKFLRRIGRFG).[21] Due to their charge density and helical conformation, these proteins domains exhibit a high affinity for calcium phosphate and therefore high adsorption on the surface of HA.

The main goals of the present work were to study the influence of SN$_A$15 on the behavior of calcium phosphate interaction when incorporated into ELR and to elucidate how the amphiphilic properties of these ELRs affect the calcium phosphate phases and morphologies generated. To this end, new hybrid recombinamer was designed, produced and characterized in which three SN$_A$15 domains were combined with the hydrophilic end of the ELR E50I60, thus resulting in the presence of SN$_A$15 on the external surface of E50I60 micelles. The effect of this ELR on calcium phosphate formations was studied in parallel with that of the ELR ((IK)2-SN$_A$15-(IK)2)3, which has three SN$_A$15 domains distributed along its monomer chain.

2. Materials and experimental methods

2.1. Recombinamer synthesis

The composition and length of monodisperse amphiphilic ELR molecule can be controlled using standard genetic engineering methods.[22] As such, sequential introduction of repetitive EL- or SN$_A$15-polypeptide-coding gene segments was carried out using the recursive directional ligation technique to form fusion genes. This method requires the construction of coding gene segments flanked at both ends with non-palindromic restriction sites. In this work, the gene segments encoding each monomer were contained in a modified version of the cloning vector pDrive (Qiagen), known as pDAll, which is characterized by the engineering of two inverted Ear I and one Sap I restriction sites into the poly-linker region. Construction of the (SN$_A$15)$_3$E50I60 sequence was verified using agarose gel electrophoresis of the restriction fragments generated after enzymatic digestion and automated DNA sequencing. Selected genes were sub-cloned into a modified version of pET-25(+) expression vector and then transformed into *E. coli* strain BLR (DE3) star (Invitrogen).

2.2. ELR production and purification

Purification was performed by inverse temperature cycling using the following procedures.[22] After lysis of *E. coli* expression colonies, the denatured materials were removed by cold centrifugation (4 °C) at 15 000 x *g* for 30 min. After that, 1 M of NaCl was added to the soluble fraction and the mixture heated for 1 h at 40 °C. Centrifugation at 40 °C was performed, and the insoluble fraction was re-suspended in cold ultrapure water, followed by cold centrifugation. The soluble fraction was subjected to two additional cycles of heating with NaCl addition and cold re-suspension. Finally, the ELR was dialyzed in ultrapure water and the final pH of the solution adjusted to about 7.4, followed by lyophilization. The resulting (SN$_A$15)$_3$E50I60 was characterized by matrix-assisted laser desorption–ionization time-of-flight (MALDI-TOF) mass spectrometry, amino-acid analysis, nuclear magnetic resonance (NMR), attenuated total reflection infrared (ATR-IR) spectroscopy and differential scanning calorimetry (DSC).

2.3. MALDI-TOF mass spectrometry

MALDI-TOF mass spectrometry was used to determine the molecular weight of ELRs. The matrix used for MALDI-TOF analysis was composed of 7.6 mg of 2,5-DHAP dissolved in 375 mL of ethanol and mixed with 125 mL of 18 mg mL^{-1} $C_6H_8O_7$•$2NH_3$ aqueous solution. Then, 1 mL from this matrix was added to the MALDI plate along with 1 mL ELR solution. The plate was dried in air and the mass spectra collected using a Bruker auto□ex speed instrument equipped with a nitrogen laser (337 nm) operating in the positive ion mode with delayed extraction.

2.4. NMR spectroscopy

Proton nuclear magnetic resonance (^{1}H NMR) spectroscopy was performed using a 400-MR NMR spectrometer (400 MHz, Agilent Technologies). 15–20 mg of the puri□ed ELR was dissolved in 600 mL of deuterated dimethyl sulfoxide (DMSO-d_6) and the spectrum measured at 25 °C. Chemical shi□s (δ) are given in ppm. Data were processed using MestReNova so□ware. DMSO-d_5 peaks at δ ¼ 2.5 ppm was used as internal reference for the ^{1}H spectra.

2.5. Amino acid analysis

Samples were hydrolysed in 6 M HCl and 2% phenol (30 min at 160 °C) and evaporated under inert atmosphere. The solid residues were re-suspended in 1 mL of 0.1 M HCl. Then, derivatizations with the OPA and FMOC chemistries were performed using an Agilent 1329A auto-sampler as reported in literature.[23] The derivatized amino acids were analysed by HPLC with UV detection using an Agilent 1200 series variable wavelength detector equipped with a G1314B detector.

2.6. ATR-IR spectroscopy

ATR-IR analyses were conducted using a BRUKER TENSOR 27, USA spectrophotometer. Solid ELR samples were placed directly on the ATR crystal for measurement. For each spectrum, a 128-scan was collected with a resolution of 2 cm^{-1} in the range 4000 to 600 cm^{-1}. Spectral manipulations were performed using the OPUS (version 4.2) so□ware (Mattson Instrument, Inc.).

2.7. DSC

A Mettler Toledo 822e differential scanning calorimeter (DSC), with liquid-nitrogen cooler and calibrated with indium, was used to calculate the T_t of the ELRs synthesized. ELR samples were dissolved in ultrapure water at a concentration of 50 mg mL^{-1} at 4 °C. Then, 20 mL of ELR solution was placed in a 40 mL sealed aluminum pan, and the same volume of ultrapure water was placed in the reference pan. Before the experiment, samples were held at 0 °C for 5 min and measurements were performed in the range 0 to 60 °C at a heating rate of 5 °C min^{-1}.

2.8. Circular dichroism (CD)

A Jasco J-815 spectropolarimeter (Jasco Inc., Easton, MD) under a constant nitrogen gas □ow was used to obtain CD spectra for ELRs. Samples were dissolved in 0.5 mM $CaCl_2$ (pH rv 7.4) at 0.05 mg mL^{-1}, and □ltered using a PVDF 0.45 mm STE: R syringe □lter at 4 °C. CD spectra were recorded at 37 °C over the wavelength range 190–260 nm, using a 0.2 cm path length quartz cell, recording a point every 0.5 nm with a scan speed of 50 nm min^{-1}.

2.9. Calcium phosphate precipitation in the presence of ELRs

When a solution of calcium cations is mixed with a solution of phosphate anions, calcium phosphate nucleation and crystallization can take place. To be able to investigate the effect of various ELRs on the reaction of calcium phosphate, the following procedure was performed. The □rst step was to dissolve ELR at the desired concentration in 10 mM solution of $CaCl_2$ at 4 °C. The sample solution was then heated to 37 °C and kept at this temperature for least 15 min (pH 7.4) under continuous magnetic stirring. A□er that, an equivolume solution of 6 mM Na_2HPO_4 at 37 °C (pH 7.4) was added to the solution to give a □nal Ca/P ratio of 1.67, similar to that found in the literature.[6,9] The calcium phosphate precipitation was studied at □nal ELRs concentrations of 0, 0.5, 1, 2, 3 and 4 mg mL^{-1}. All reagents used for preparation of calcium and phosphate solutions were obtained from Sigma Aldrich and used without further puri□cation. The temperature was controlled during the reaction using thermo-jacketed vessels coupled to a thermostatic bath (Huber CC2).

The calcium phosphate reaction was monitored with the help of an electrical conductivity probe (Crison MM41). The initial time of reaction (t ¼ 0) was taken when the phosphate solution added to the mixture. All conductivity pro□les were analyzed and the induction time, de□ned as the time taken for metastable transient phases to transform into more stable phases, was determined.[9,24]

2.10. X-ray diffraction (XRD)

The composition of calcium phosphate precipitated in the absence or presence of ELRs was analyzed by X-ray diffraction. Samples were isolated by centrifugation, washed two times using ultrapure water and dried at 37 °C. The white precipitate was then ground in an agate mortar prior to XRD analysis. XRD patterns were recorded on a Bruker D8 Discover A25 equipment using CuK_a radiation (λ ¼ 1.5406 Å) and a silicon sample holder. The step size was 0.02°. Crystallographic identi□cation of the examined phases was compared with the PDF 01-072-1243.

2.11. Energy dispersive X-ray spectroscopy (EDX)

The Ca/P ratio of the calcium phosphate precipitated a□er centrifugation, washing and drying, was determined by energy dispersive X-ray spectroscopy (EDAX Genesis with an Apollo SDD detector, 10 mm).

2.12. Transmission electron microscopy (TEM)

TEM specimens were prepared by soaking a 300 mesh carbon-coated copper grid in the required solution for the required time. The grid was then removed and blotted immediately to remove the excess of liquid, and air-dried. Electron microscopy and diffraction were performed using a JEOL-JEM 2200FS system

operating at 200 kV and equipped with an energy dispersive X-ray (EDX) analysis detector. The microscope was equipped with an in-column Ω-type energy filter. Zero-loss images were recorded to increase contrast. X-ray spectra were acquired in scanning transmission electron microscopy (STEM) mode using an Oxford INCA EDX system. The live counting time was 100 s.

3. Results and discussion

3.1. Hybrid elastin-like-statherin recombinamers

The amino acid sequence of the different constructs E50I60, $(SN_A15)_3$E50I60, IK24 and ((IK)2-SN_A15-(IK)2)3 are shown in Table 1. E50I60, (IK)24 and ((IK)2-SN_A15-(IK)2)3 were synthesized and characterized as reported previously in the literature.[19,20,25] The transition temperature (T_t) of the ELR E50I60 was exploited to purify the whole $(SN_A15)_3$E50I60 hybrid molecule under water-based and mild conditions. The final $(SN_A15)_3$E50I60 product was characterized by SDS-page analysis, MALDI-TOF mass spectrometry, ^{1}H NMR, amino-acid analysis and ATR-IR spectroscopy (ESI: Fig. S1–S4 and Tables S1 and S2†), which proven the correctness and purity of the biosynthetic process in terms of sequence and molecular mass. DSC experiments were performed in order to check the T_t of the ELR $(SN_A15)_3$E50I60 (Fig. S5†).

As the secondary structure of polypeptides has a remarkable influence on controlling the mineralization process,[4,10,26] CD was used as a spectroscopic technique to study the conformation of ELRs shown in Table 1. Calcium phosphate interaction in the presence of these ELRs was then examined by monitoring the electrical conductivity (σ) as a function of time. The induction time (I_t), defined as the time at which a stable solid phase starts to form, was also determined. The formed calcium phosphates were characterized by XRD. Moreover, the morphologies of the calcium phosphate species formed were observed by TEM and characterized by electron diffraction and EDX. To this end, the reaction conditions were chosen carefully to be able to visualize the amorphous phase transformations in an adequate time frame.

3.2. Circular dichroism spectroscopy (CD)

CD has been used to analyze the basic secondary structure of polypeptide, α-helix, β-sheet, β-turns and random coils.[27–30] Fig. 1 shows the CD spectra recorded for the ELRs, all of which exhibit one positive and two negative peaks. The negative peaks centered at 197, 199 and 200.5 nm are attributed to the random coil conformations, whereas the negative peak centered at 223 nm and the positive peak at 209–212 nm are assigned to type II β-turns.[28–30] The Mean Residual Ellipticity (MRE) of the characteristic random coil peak of these ELRs is higher than that found for an ideal random coil (-40 000 deg cm^2 dmol^{-1}).[29,30] This is due to the presence of β-turn conformations stemming from the hydrophobic (VPGIG) block.

Fig. 1A shows that the center of the random coil peak is shifted from 197 to 199 nm, with its amplitude changing from -3670 to -3463 deg cm^2 dmol^{-1} when SN_A15 is recombined with the E50I60 monomer chain. In addition, the amplitude of the β-turn peak alters from -2581 to -3019 deg cm^2 dmol^{-1}. A similar behavior can be observed in Fig. 1B for IK24 and ((IK)2-SN_A15-(IK)2)3 in which the characteristic random coil peaks are found at 197 and 200.5 nm with MRE amplitudes of -6421 and -4436 deg cm^2 dmol^{-1}, respectively. There is no shift in the amplitude of the β-turn peak can be seen.

3.3. Formation of nanofibre-like hydroxyapatite structure controlled by $(SN_A15)_3$E50I60

Electrical conductivity measurements performed during the calcium phosphate reaction in the absence/presence of E50I60 and $(SN_A15)_3$E50I60 are shown in Fig. 2A. The profiles presented clearly exhibit three regions after phosphate addition. Region I corresponds to the initial precipitation of a metastable calcium phosphate phase, which is an amorphous phase that is susceptible to rapid transformation (region II) into a secondary stable precipitate (region III).[9,24] It can be seen from Fig. 2B that E50I60 does not significantly affect the I_t, which remains at

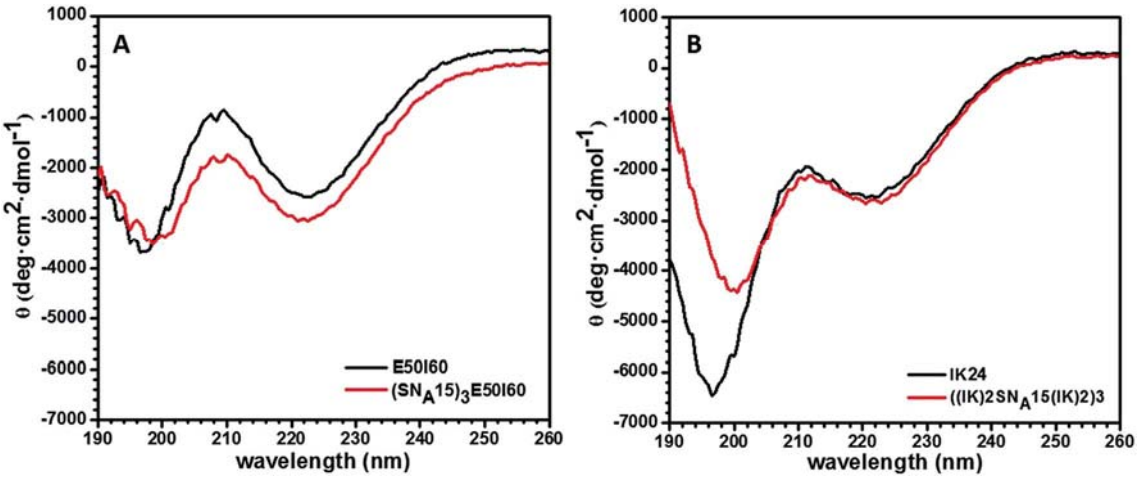

Fig. 1 CD of ELRs at 0.05 mg mL^{-1} dissolved in 0.5 mM $CaCl_2$ (37 °C), (A) E50I60 and $(SN_A15)_3$E50I60, and (B) IK24 and ((IK)2-SN_A15-(IK)2)3.

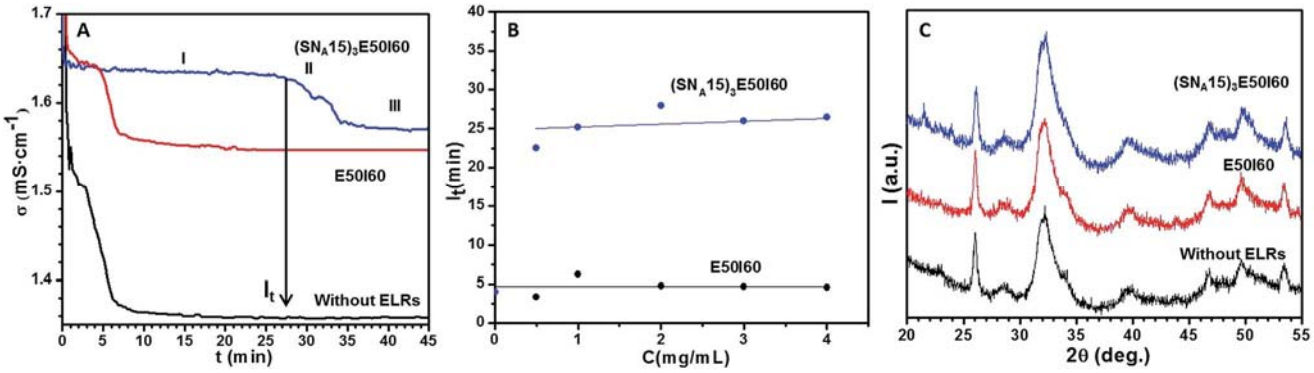

Fig. 2 (A) Electrical conductivity profiles measured by mixing 3 mL of 10 mM $CaCl_2$ and 3 mL of 6 mM Na_2HPO_4 at 37 °C (pH 7.4) in the presence of E50I60 (red curve) and $(SN_A15)_3$E50I60 (blue curve) at 2 mg mL^{-1}. The conductivity profile (black curve) in the absence of these ELRs is included for comparison. (B) I_t as a function of these ELR concentrations. Lines are drawn to allow the changes to be seen more clearly. (C) XRD patterns of the precipitates after I_t (region III) in the presence of E50I60 (red curve) and $(SN_A15)_3$E50I60 (blue curve) at 2 mg mL^{-1}. The XRD pattern of the precipitate formed in the absence of ELRs (black curve) is included for comparison.

about 5 min, even with increasing concentration. This value is similar to that obtained for the control sample in the absence of ELRs. In contrast, $(SN_A15)_3$E50I60 delays the secondary precipitation with a nearly constant I_t of around 25 min.

The precipitates formed a□er I_t (region III) were examined using XRD (Fig. 2C) con□rming the presence of HA (PDF 01-072-1243). The peaks are broad accounting for the poorly crystalline nature of the precipitates. The Ca/P ratios of the precipitates in the presence of 2 mg mL^{-1} E50I60 and $(SN_A15)_3$E50I60 were 1.45 ± 0.02 and 1.46 ± 0.02, respectively, and that of HA formed in the absence of ELRs was 1.45 ± 0.02. These ratios are assigned to calcium de□cient HA.[31-33]

The morphologies and phases of the formed calcium phosphate a□er I_t (region III) are shown in Fig. 3. In the absence of ELRs, the formed calcium phosphate is mostly composed of plate-like crystals, as shown in Fig. 3A. Moreover, the electron-diffraction pattern shown in the inset to the □gure exhibits a crystal lattice corresponding to the HA phase consistent with the XRD results. The addition of E50I60 does not seem to signi□cantly alter the morphology of the HA (Fig. 3B), whereas a completely different structure consisting of polycrystalline nano□bre-like HA aggregates (Fig. 3C) is formed in the presence of $(SN_A15)_3$E50I60.

3.4. Formation of neuron-like morphologies controlled by ((IK)2-SN_A15-(IK)2)3

Fig. 4A shows the electrical conductivity pro□les for the mixed calcium phosphate solutions in the absence/presence of (IK)24 and ((IK)2-SN_A15-(IK)2)3. Fig. 4B shows that I_t is independent of the presence of the former ELR, remaining at about 5 min even upon increasing the concentration. In contrast, the latter ELR delays secondary precipitation with a steady, concentration-dependent, increase in I_t up to about 37 min at 4 mg mL^{-1}. The XRD patterns (Fig. 4C) of the precipitates formed in the absence/presence of (IK)24 and ((IK)2-SN_A15-(IK)2)3 are assigned to poorly crystalline HA phase (PDF 01-072-1243). The Ca/P ratio determined by EDX in the presence of 2 mg mL^{-1} of (IK)24 and ((IK)2-SN_A15-(IK)2)3 is 1.43 ± 0.02 and 1.47 ± 0.08 respectively, which is attributed to calcium de□cient HA.[31-33]

Fig. 5B shows the morphologies and phases of the calcium phosphate formed in the presence of IK24, con□rming the formation of plate-like HA crystals similar to those observed in the control sample without ELRs. In contrast, for ((IK)2-SN_A15-(IK)2)3 neuron-like structures were mostly observed (Fig. 5C and D). The cores of these neurons were examined by EDX revealing the presence of calcium and phosphate with Ca/P $_{rv}$1.14 (Fig. S6†). At a concentration of 0.5 mg mL^{-1}, the neuron-like

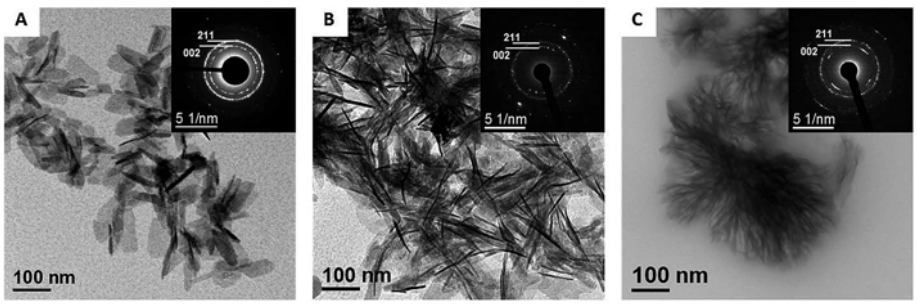

Fig. 3 TEM showing the morphology of the calcium phosphate obtained after I_t and their corresponding electron-diffraction patterns: (A) in the absence of ELRs and in the presence of (B) 2 mg mL^{-1} E50I60 and (C) 2 mg mL^{-1} $(SN_A15)_3$E50I60. Some planes consistent with the HA crystal lattice can be observed in the electron-diffraction patterns (inset).

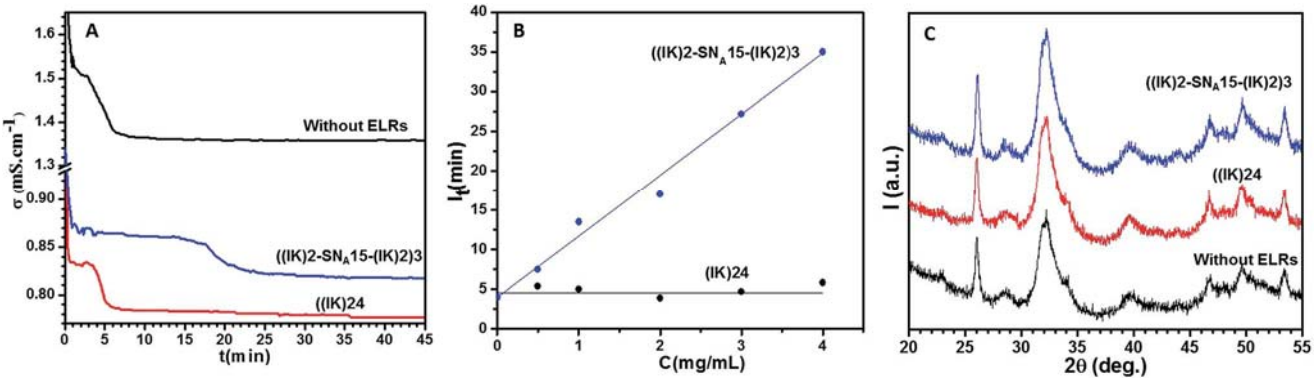

Fig. 4 (A) Electrical conductivity profiles measured by mixing 3 mL of 10 mM $CaCl_2$ and 3 mL of 6 mM Na_2HPO_4 at 37 °C (pH 7.4) in the presence of IK24 (red curve) and ((IK)2-SN_A15-(IK)2)3 (blue curve) at 2 mg mL^{-1}. The conductivity profile (black curve) in the absence of these ELRs is included for comparison. (B) I_t as a function of IK24 and ((IK)2-SN_A15-(IK)2)3 concentration. Lines are drawn to allow the changes to be seen more clearly. (C) XRD patterns of the precipitates after I_t (region III) in the presence of IK24 (red curve) and ((IK)2-SN_A15-(IK)2)3 (blue curve) at 2 mg mL^{-1}. The XRD pattern of the precipitate formed in the absence of ELRs (black curve) is included for comparison.

morphology has a core of about 40–50 nm and thin nano□laments about 5–10 nm in width and 150–200 nm in length. Upon increasing the concentration to 2 mg mL^{-1}, the □laments become shorter (about 100–150 nm) whereas the core becomes larger (about 90–120 nm), thus forming a mesostructured ACP/((IK)2-SN_A15-(IK)2)3. High resolution TEM analyses demonstrate that the cores and □laments do not exhibit any crystallite formation. Electron-diffraction analyses of the neuron-like cores con□rm their amorphous structure (inset of Fig. 5C). This contrasts with the XRD patterns that indicate the presence of an additional phase: poorly crystalline HA. The presence of this phase is due to spontaneous precipitation and is not controlled by ((IK)2-SN_A15-(IK)2)3.

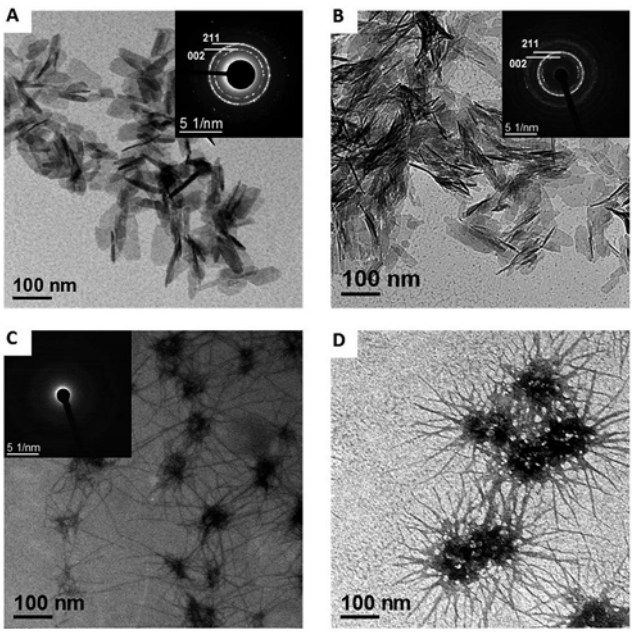

Fig. 5 TEM showing the morphology of the calcium phosphate obtained after I_t (region III) and their corresponding electron-diffraction patterns: (A) in the absence of ELRs and in the presence of (B) 0.5 mg mL^{-1} (IK)24, (C) 0.5 mg mL^{-1} ((IK)2-SN_A15-(IK)2)3, and (D) 2 mg mL^{-1} ((IK)2-SN_A15-(IK)2)3.

Although the self-assembling process of hybrid biomaterials in the present work has the merit of mild reaction conditions, the main disadvantage associated to this synthesis route is precisely the low temperature and the mild reaction conditions that o□en leads to precipitation of secondary phases (*i.e.* HA). Many alternative routes can be used to overcome this drawback (hydrothermal, sonochemical or combustion techniques among others) but at the cost of sacri□cing the mild reaction conditions inherent to biomimetic synthesis routes.[32,33] However, in spite of the presence of HA for ((IK)2-SN_A15-(IK)2)3, the effect of this recombinamer in the modulation of calcium phosphate precipitation is clear.

3.5. Mechanisms controlling calcium phosphate formation under the in□uence of self-assembling ELRs as organic additives

Organic additives are well known to modulate amorphous-to-crystalline calcium phosphate transformations and to in□uence the stabilization of amorphous phases.[1,2,5,6,9,34,35] This can be achieved by the presence of locally highly charged areas on the organic molecules that can induce electrostatic and hydrogen-bonding interactions with the calcium and phosphate ions during the mineralization process. The hydrophobic constituent of these organic matrixes can act as an architectural framework, whereas the hydrophilic constituents are directly involved in controlling mineral nucleation and growth. Due to the strong binding interactions between organic and inorganic phases, aggregates composed of hybrid primary particles with metastable ACP can be generated.[1,2,5,6,9,34,35] This metastable ACP can slowly crystallize inside these aggregates. For example, in the present work, the organic additives $(SN_A15)_3$E50I60 and ((IK)2-SN_A15-(IK)2)3 can delay I_t, whereas the other organic additives E50I60 and (IK)24 cannot. Consequently, SN_A15 has a marked ability to control the mineralization process of calcium phosphate. Moreover, two different morphologies, namely □bre- and